Nanoscale

PAPER

View Article Online
View Journal | View Issue

Cite this: *Nanoscale*, 2019, **11**, 19497

Prussian blue analogue nanoenzymes mitigate oxidative stress and boost bio-fermentation†

Renwu Zhou, *‡[a,b,c] Peiyu Wang,‡[a,b] Yanru Guo,‡[d] Xiaofeng Dai,[e] Shaoqing Xiao,[f] Zhi Fang,*[g] Robert Speight,[a] Erik W. Thompson,[a,b] Patrick J. Cullen[c] and Kostya (Ken) Ostrikov[a,b]

Received 11th June 2019,
Accepted 12th September 2019

DOI: 10.1039/c9nr04951g

rsc.li/nanoscale

Oxidative stress in cells caused by the accumulation of reactive oxygen species (ROS) is a common cause of cell function degeneration, cell death and various diseases. Efficient, robust and inexpensive nanoparticles (nanoenzymes) capable of scavenging/detoxifying ROS even in harsh environments are attracting strong interest. Prussian blue analogues (PBAs), a prominent group of metalorganic nanoparticles (NPs) with the same cyanometalate structure as the traditional and commonly used Prussian blue (PB), have long been envisaged to mimic enzyme activities for ROS scavenging. However, their biological toxicity, especially potential effects on living beings during practical application, has not yet been fully investigated. Here we reveal the enzyme-like activity of FeCo-PBA NPs, and for the first time investigate the effects of FeCo-PBA on cell viability and growth. We elucidate the effect of the nanoenzyme on the ethanol-production efficacy of a typical model organism, the engineered industrial strain *Saccharomyces cerevisiae*. We further demonstrate that FeCo-PBA NPs have almost no cytotoxicity on the cells over a broad dosage range (0–100 μg mL^{-1}), while clearly boosting the yeast fermentation efficiency by mitigating oxidative stress. Atmospheric pressure cold plasma (APCP) pretreatment is used as a multifunctional environmental stress produced by the plasma reactive species. While the plasma enhances the cellular uptake of NPs, FeCo-PBA NPs protect the cells from the oxidative stress induced by both the plasma and the fermentation processes. This synergistic effect leads to higher secondary metabolite yields and energy production. Collectively, this study confirms the positive effects of PBA nanoparticles in living cells through ROS scavenging, thus potentially opening new ways to control the cellular machinery in future nano-biotechnology and nano-biomedical applications.

Introduction

Reactive oxygen species (ROS), derived from metabolic processes in living organisms, are important intermediates of cellular signalling processes and intracellular functions.[1–3] Overproduction and/or dysregulation of ROS, especially the highly reactive ones such as hydrogen peroxide (H_2O_2) and superoxide radicals ($^{\bullet}O_2^-$), causes oxidative stress in biological systems, directly contributing to the damage to cellular biomolecules, and is linked to the occurrence of various diseases and the degeneration or loss of cell functions.[4–6] Methods and agents capable of scavenging ROS and maintaining the balance between ROS generation and removal have high therapeutic and economic values.[6–8]

Natural antioxidant enzymes in cells such as superoxide dismutase (SOD) and catalase establish protective barriers for cells by detoxifying ROS and reducing damage from oxidative stress.[9–11] However, the applications of natural enzymes are much impeded by their inherent unwelcome properties that make it difficult to achieve desirable activities, such as lack of stability and specific requirements (pH, temperature and even the existence of net inhibitor), in addition to high cost and issues with large-scale production.[12–14] Recent decades have witnessed the fast development of emerging artificial enzymes, especially those based on inorganic nanomaterials (also called nanoenzymes). These nanoenzymes include noble metals, metal oxides, and carbon materials featuring not only natural

[a]*Institute of Health and Biomedical Innovation, School of Chemistry, Physics and Mechanical Engineering, Science and Engineering Faculty, Queensland University of Technology, Brisbane QLD 4000, Australia. E-mail: zhourenwu2015@163.com*
[b]*Translational Research Institute, Brisbane, QLD 4102, Australia*
[c]*School of Chemical and Biomolecular Engineering, The University of Sydney, NSW 2006, Australia*
[d]*Beijing National Laboratory for Molecular Sciences (BNLMS), College of Chemistry and Molecular Engineering, Peking University, Beijing 100871, China*
[e]*Wuxi School of Medicine, Jiangnan University, 214122, China*
[f]*Engineering Research Center of IoT Technology Applications (Ministry of Education), Department of Electronic Engineering, Jiangnan University, Wuxi 214122, China*
[g]*College of Electrical Engineering and Control Science, Nanjing Tech University, Nanjing 210009, China. E-mail: myfz@263.net*

†Electronic supplementary information (ESI) available. See DOI: 10.1039/C9NR04951G

‡Equal contribution

enzyme-like activities but also advantages such as excellent stability and ease of synthesis.[15–19]

Prussian blue (PB, $KFe^{III}[Fe^{II}(CN)_6]$) is a well-known and easily available nanomaterial widely used in magnetics, photo- and electrochemistry, and biomedicine.[20–22] Evidence suggests that PB has inconspicuous toxicity towards a variety of cell types and can harmlessly pass through the body due to its high binding affinity for cyanide ions.[23] Shokouhimehr *et al.* reported that PB is biocompatible for cellular imaging and drug delivery with high stability and insignificant intracellular production of ROS.[24] Zhang *et al.* also discovered that PB nanoparticles (PB NPs) could effectively scavenge reactive oxygen species (ROS). The ROS scavenging effect of PB NPs is attributed to their affinity for hydroxyl radicals (•OH) and ability to mimic three antioxidant enzymes including peroxidase (POD), catalase (CAT), and superoxide dismutase (SOD).[23] Meanwhile, the cyanometalate structural analogues of PB (usually termed PB analogue nanoparticles, PBA NPs, $A_xM'[M''(CN)_6]_y{\cdot}nH_2O$, A: alkaline metal; M: transition metal; $0 \le x \le 2$; $y \le 1$) have attracted strong attention through many encouraging results in electrocatalysis, molecular magnetism, hydrogen storage, solid cells, and other areas.[25] Recently, PBA NPs have been found to effectively mimic the functions of ROS-scavenging enzymes, thus showing promise in biotechnology applications.[26] However, the biological effects of PBA NPs, especially their cytotoxicity and ROS scavenging ability, remain largely unexplored.

To fill the gap, in this study, a typical PB analogue, FeCo-PBA, is synthesized and its enzyme-like activities are examined both extracellularly and intracellularly (Fig. S1, ESI†). The FeCo-PBA particles are then used in the yeast fermentation process for enhancing ethanol production and providing new insights for potential real-world applications. *Saccharomyces cerevisiae* is a widely used and well-studied unicellular eukaryote facilitating beverage fermentation. Recent findings suggest that in ethanol fuel production, both the viability and fermentative ability of the yeast are negated by ROS generation during fermentation. The problem escalates when the produced ethanol accumulates and other stress factors such as pH, temperature, osmotic pressure and fermentation inhibitors come into play.[27,28] Substantial efforts, especially those based on complex and costly genetic engineering, have been made to improve ethanol and ROS tolerance and enhance the metabolic activity of *S. cerevisiae* to maximize the benefits in bio-fermentation.[29,30] Here, a unique physicochemical treatment, atmospheric pressure cold plasma (APCP),[31,32] is applied to stress the yeast cells and validate the anti-oxidative effects of the PBA in a simulated ROS-containing environment (Fig. S2, ESI†).

Results and discussion

Characterization of the synthesized FeCo-PBA NPs

The XRD patterns in the 2θ range from 10° to 80° of FeCo-PBA nanoparticles are presented in Fig. 1(a). All the main characteristic diffraction peaks could be indexed to FeCo-PBA (JCPDS

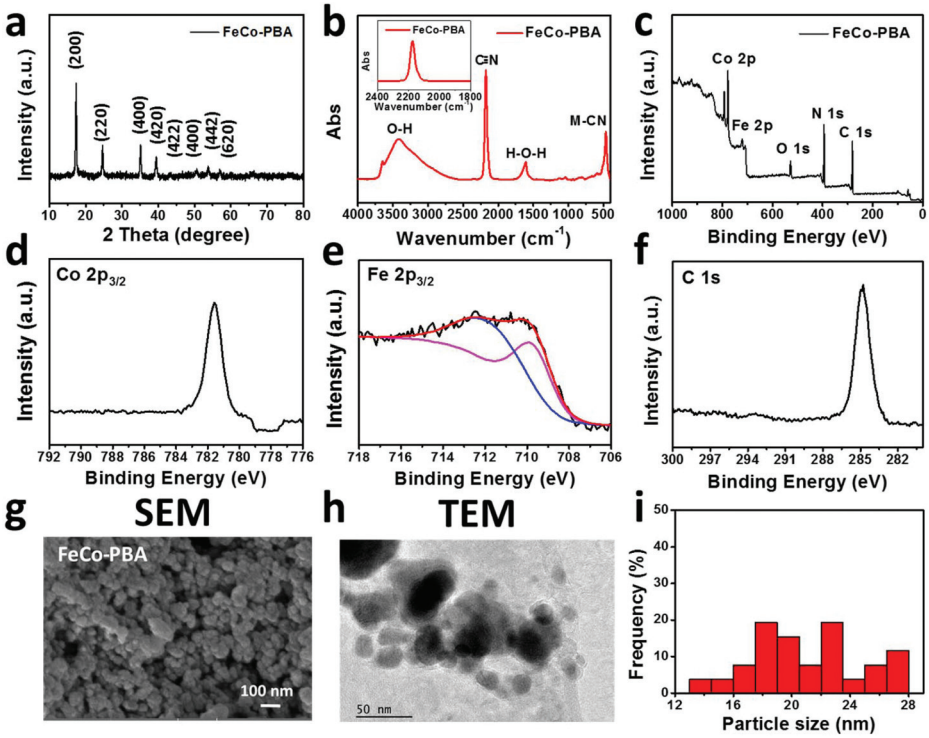

Fig. 1 Characterization of the FeCo-PBA NPs. (a) XRD pattern of FeCo-PBA NPs. (b) FTIR spectra of FeCo-PBA NPs. (c) XPS spectra of FeCo-PBA NPs. (d) Co $2p_{3/2}$ XPS spectra. (e) Fe $2p_{3/2}$ XPS spectra. (f) C 1s XPS spectra. (g) The SEM image of FeCo-PBA NPs. (h) The TEM image of FeCo-PBA NPs. (i) DLS analysis of the nanoparticles.

card no. 89-3736), which is in good agreement with the result of simulated XRD of the face-centred cubic (fcc) phase of $Fe_3[Co(CN)_6]_2{\cdot}nH_2O$. IR spectroscopy presents the bonding information of FeCo-PBA nanoparticles. The characteristic peaks located at 2175 cm^{-1} are attributed to the C≡N triple bond stretching mode including the vibrations of Fe(III)–CN–Co(II) and Fe(II)–CN–Co(III) due to electron-transfer processes.[33] X-ray photoelectron spectroscopy (XPS) is employed to investigate the valence state of FeCo nanoparticles. Fig. 1(c) shows the overall XPS survey spectrum of the sample. Five elements including carbon, oxygen, nitrogen, cobalt and iron are identified. The XPS spectra of Co 2p and Fe 2p show two doublets of 1/2 and 3/2. Two peaks of Co $2p_{3/2}$ with the binding energies located at 781.5 eV are attributed to the existence of $[Co(CN)_6]^{3-}$. Similarly, for Fe $2p_{3/2}$, two characteristic peaks at 711.8 eV and 710.1 eV could be assigned to Fe(III) and Fe(II).[34] Fig. 1(g)–(i) show the morphological structures of FeCo-PBA nanoparticles. The scanning electron microscopy (SEM) image (Fig. 1(g)) reveals that the FeCo PBA samples are composed of numerous crystalline nanoparticles with a sphere-like morphology. The transmission electron microscopy (TEM) image (Fig. 1(h)) and the corresponding size distribution histograms show that the diameter of the spherical particles is approximately 10–30 nm. The stability of FeCo-PBA NPs is evaluated using UV-vis absorption spectroscopy. The results show that the optical density at 600 nm (OD_{600}) of the nanoparticle suspension does not decrease with time in aqueous solution (Fig. S3, ESI†), indicating that there is no sedimentation or obvious agglomeration of particles.

Catalase and SOD mimicking activity of FeCo-PBA NPs

H_2O_2 and $^{\bullet}O_2^-$ are two ROS representatives widely produced by different cellular metabolic processes, and both are highly destructive once their amount exceeds the antioxidant capacity of the cells themselves.[15] To understand the anti-ROS ability of FeCo-PBA NPs, solutions containing H_2O_2 or $^{\bullet}O_2^-$ are prepared and then combined with NPs, as well as with natural enzymes or commercial antioxidants for comparison. ROS scavenging is quantified by using fluorescent probes. In the presence of FeCo-PBA NPs, the fluorescence intensities significantly decrease just as in the case of trolox/tempol and natural catalase/SOD, illustrating that H_2O_2 and $^{\bullet}O_2^-$ can be effectively eliminated, and directly proving that FeCo-PBA NPs possess both catalase- and SOD-like activity. Specifically, more than 75% of H_2O_2 can be eliminated by using 20 μg mL^{-1} of pristine FeCo-PBA NPs (without heat pretreatment), the scavenging activity of which is considerably better than those of 100 μM synthetic trolox (67.4%) and 10 U mL^{-1} of catalase (65.8%). Although lowering the dose of NPs will lead to an expected reduced elimination, 10 μg mL^{-1} of NPs presented H_2O_2 detoxifying ability comparable to the natural enzyme. Additionally, the multifunctional ROS probe CellROX® Orange can also be oxidized by $^{\bullet}OH$, the product of H_2O_2, catalysed by transition metal compounds. The significant decrease in the fluorescence intensity in the NP-added groups thus suggests that the H_2O_2 scavenging activity of FeCo-PBA NPs does not depend on the generation of OH radicals, which is consistent with the previous research using PB NPs.[26] The elimination of 58.3 and 80.3% of $^{\bullet}O_2^-$ radicals can be witnessed when 10 and 20 μg mL^{-1} of FeCo-PBA NPs are used as scavengers, respectively. Both these figures are lower than those obtained by using 2 U mL^{-1} of the natural $^{\bullet}O_2^-$ antidotal enzyme SOD (more than 90%), but either comparable or significantly higher than those for 1 mM tempol (~60%). Our results thus suggest that FeCo-PBA NPs also possess SOD-like activity and this activity is dose-dependent. Hence, the effective elimination of SOD can be achieved by optimizing the dosage of SOD according to specific requirements of applications.

It has been reported that H_2O_2 can be oxidized or reduced through two electron transfer channels in PB, high-spin $Fe^{3+/2+}$ and low-spin $Fe(CN)_6^{3-/4-}$, respectively (*via* reactions (1) and (2)).[23] When the electrode potential is lower than 0.7 V, the electron transfer of high-spin $Fe^{3+/2+}$ plays the main role, whereas low-spin $Fe(CN)_6^{3-/4-}$ is predominant when the electrode potential reaches 0.9 V. In addition, with these cyanide-bridged bimetallic tridimensional coordination networks, PBNPs can also efficiently quench $^{\bullet}O_2^-$, displaying SOD-like activity (reaction (3)).[23] As shown in the framework structure of an ideal cubic PBA (Fig. 2(a)), its composition is $CoFe(CN)_6$, and the (Fe + Co)/CN molar ratio is 1/3. Due to a reversible metal-to-metal electron transfer process between the cobalt and iron centers, switching between paramagnetic (Fe^{III}_{LS}–CN–Co^{II}_{HS}) and diamagnetic (Fe^{II}_{LS}–CN–Co^{III}_{LS}) configurations (Fig. 2(b); with LS: low spin and HS: high spin), PBA NPs can also display ROS scavenging abilities for controlling ROS-induced cell damage.

$$H_2O_2 \rightarrow O_2 + 2e^- + 2H^+ \quad (1)$$

$$H_2O_2 + 2e^- + 2H^+ \rightarrow 2H_2O \quad (2)$$

$$2{\bullet}OOH \xrightarrow{SOD/PBNPs} H_2O_2 + O_2 \quad (3)$$

In order to test the thermal stability of the ROS detoxifying ability induced by FeCo-PBA NPs (especially when they are subjected to a higher temperature), which may determine their potential applications, all ROS scavengers (in solutions) used in this study (FeCo-PBA NPs, synthetic trolox/tempol, and natural enzymes) are pre-treated at 80 °C for 1 h before testing

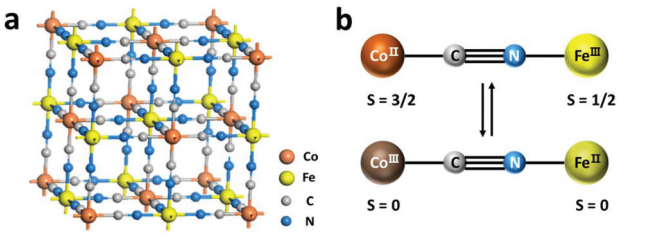

Fig. 2 Schematic representation of a Fe/Co Prussian blue network and its interconversions. (a) The structure of FeCo-PBA with the composition $Co_3(Fe(CN)_6)_2$. (b) Interconversion between the paramagnetic (Fe^{III}_{LS}–CN–Co^{II}_{HS}) and diamagnetic (Fe^{II}_{LS}–CN–Co^{III}_{LS}) electronic configuration due to ROS induced metal-to-metal electron transfer processes.

Table 1 Catalase mimicking activity of FeCo-PBA NPs

	H_2O_2 elimination (%)			$^{\bullet}O_2^-$ elimination (%)	
Treatment	Pristine[a]	80 °C[a]	Treatment	Pristine[a]	80 °C[a]
H_2O_2[b]	0.0	0.0	X + XO[b]	0.0	0.0
H_2O_2 +trolox	67.4 ± 2.5	34.2 ± 2.7	X + XO + tempol	60.1 ± 4.6	40.3 ± 3.5
H_2O_2 + catalase	65.8 ± 1.7	20.5 ± 3.4	X + XO + SOD	90.2 ± 2.8	6.2 ± 5.2
H_2O_2 + 10 μg mL^{-1} FeCo-PBA NPs	59.5 ± 3.2	57.3 ± 2.2	X + XO + 10 μg mL^{-1} FeCo-PBA NPs	58.3 ± 2.9	60.1 ± 1.9
H_2O_2 + 20 μg mL^{-1} FeCo-PBA NPs	79.9 ± 1.1	80.8 ± 1.9	X + XO + 20 μg mL^{-1} FeCo-PBA NPs	80.3 ± 2.2	80.2 ± 3.0

[a] Pristine for scavengers used directly; 80 °C refers to the pretreatment temperature. [b] The elimination of the groups without any ROS-scavengers was defined as 0.0% for comparison.

their H_2O_2 and $^{\bullet}O_2^-$ elimination efficiencies. As detailed in Table 1, the natural enzymes, the functions of which are usually temperature-dependent, lost most of their ROS scavenging activities, especially in the case of SOD. The abilities of both trolox and tempol can be preserved by around 50% after thermal pre-treatment. And yet, it is encouraging to see that FeCo-PBA NPs show significantly better thermal stability with almost all the elimination efficacy retained. Similar results were also reported in research studies using Mn-based nanoparticles,[35] further highlighting the feasibility of the nanoenzyme operation at higher temperatures.

Cell viability and growth of *S. cerevisiae* cells with FeCo-PBA NPs

To investigate the possible toxicity of the synthesized FeCo-PBA nanoparticles against yeast cells (*S. cerevisiae*), we firstly perform the staining assay on this yeast under the treatment of FeCo-PBA NPs at different concentrations. The results show that these nanoparticles have no obvious inhibition effects on *S. cerevisiae* cells (Fig. 3(a) and Fig. S4, ESI†), and that the uptake of NPs does not lead to an increase of intracellular ROS (Fig. S5, ESI,† tested using the CellROX® Orange ROS kit after the cells were co-cultured with NPs for 1 h). In other words, FeCo-PBA nanoparticles are biocompatible and exhibit low toxicity to yeast cells even when the dosage is 100 μg mL^{-1}. Cell growth of *S. cerevisiae* in YPD media containing FeCo-PBA at different concentrations is then monitored using a micro-plate reader for 24 h (Fig. S6, ESI†). The results show that the addition of FeCo-PBA enhances the proliferation of yeast cells. This enhancement is dose-dependent. Indeed, 5 μg mL^{-1} of FeCo-PBA increases cell proliferation by 3.5% while 100 μg mL^{-1} increases it by 10.8% compared to the control.

Cell growth is accompanied by metabolic processes and the generation of ROS. The existence of exotic ROS scavengers would then inhibit the accumulation of these ROS and the emergence of oxidative stress in cells. These results indicate that FeCo-PBA can play a positive role during cell growth, indicating its potential for application as promoters of targeted products in bio-engineering and drug delivery vectors in biomedicine. Higher concentrations of nanoparticles (within appropriate ranges) in the culture solutions are easily taken up by cells, effectively modifying the metabolic activity of the cells.[36] The cellular uptake of FeCo-PBA NPs in *S. cerevisiae* cells is then studied by inverted confocal laser microscopy (Olympus FV3000) with the excitation wavelength at 512 nm and the fluorescence emission maximum at 600 nm. FeCo-PBA NPs emit green fluorescence, which makes them easy to detect inside the cells. From the confocal images (Fig. 3(b)), it is confirmed that the FeCo-PBA NPs can enter the cells. Moreover, the cellular uptake of the nanoparticles is improved in a dose-dependent manner as seen in Fig. 3(c), suggesting that the fluorescence intensity is proportional to the NP concentration.

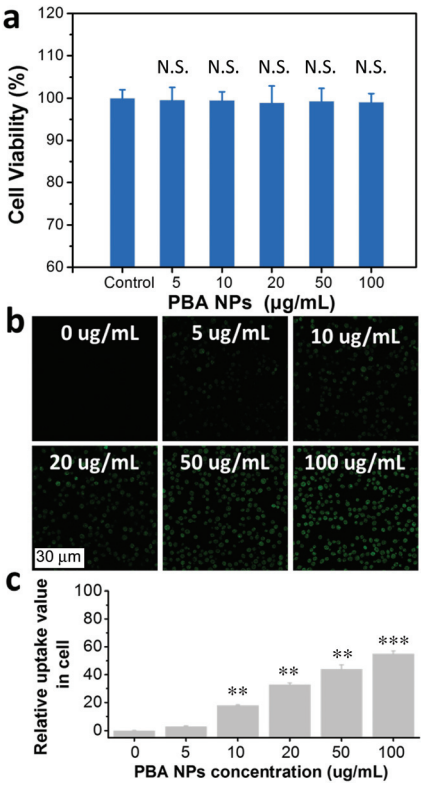

Fig. 3 (a) Cell viability of *S. cerevisiae* under different concentrations of PBA NPs. (b) and (c) Cellular uptake of PBA NPs by *S. cerevisiae* under different concentrations of PBA NPs. *S. cerevisiae* cells were incubated in YPD medium containing PBA NPs with the indicated concentrations (5–100 μg mL^{-1}). Cell viability was assessed *via* the MB staining method. NPs uptake level was expressed by relative fluorescence intensity. The data points and error bars represent the averages and standard deviations from three independent measurements, respectively.

Plasma as a cellular ROS stressor and for enhancing the cellular uptake of FeCo-PBA NPs

In order to further validate the ROS scavenging ability of the PBA NPs in cells, APCP is employed to pre-treat the yeast cells. APCP is a multi-modal stressor inducing environments rich in highly reactive species and UV photons with mild heat, well known for its biological activity and suitable for sterilization, disinfection and other biomedical applications.[37–40] Longer cell processing times are expected to produce more plasma-related effects, leading to higher cell death rates (Fig. S7, ESI†). In particular, with plasma exposure for 1 min, the cell viability of *S. cerevisiae* decreases to 91.2% and further falls to 58.5% when the plasma exposure extends to 10 min. More details about the effects of APCP on the cell viability and growth of *S. cerevisiae* can be found in our previous studies.[41] Since the main purpose of the plasma treatment here is to act as a multi-functional stressor for ROS generation inside the cells, the treatment time is chosen to be 1 min. Under such conditions, a certain amount of reactive species can be delivered into the cells, without any significant cell death effects (*i.e.*, retaining cell viability >90%). As seen in Fig. 4(a) and (b), 1 min of APCP treatment significantly increases the intracellular ROS levels 4 times (from <4 to >16 RFU). Afterwards, the increase in the ROS levels would be much lower and the ROS might even get totally eliminated if the treated cells are cultivated in FeCo-PBA containing broths (containing FeCo-PBA above 20 μg mL^{-1}) for a short time (1 h), directly confirming the cellular ROS scavenging ability of the PBA NPs.

It has been previously confirmed that plasma treatment can modify cell membranes, especially their structure and permeability.[31,42] As indicated in the SEM images (Fig. S8, ESI†), the plasma untreated *S. cerevisiae* cells are round, with a spherical shape. After APCP exposure for 1 min, the cell morphology changes to a rough surface. Indeed, a suitable dose of the plasma exposure with a weak electro-magnetic field can enlarge the pores on the surface, thus enhancing cell permeability. With longer plasma exposure times, cell surface roughness gradually increased. After 10 min of exposure, the cell structure is significantly altered with the cells appearing significantly damaged.

The observed changes in the cell membranes are correlated to the significant boost in the cellular uptake of the FeCo-PBA particles (Fig. 4(c) and (d)). Compared to the NP uptake without the plasma pre-treatment (Fig. 3), considerably more particles can pass through the cell membrane. This effect is confirmed by the higher green fluorescence intensity of the cells when the same dose of PBA is applied. For example, the NP uptake value of plasma-treated yeast cells with 20 μg mL^{-1} of FeCo-PBA is comparable to that of the untreated cells with 100 μg mL^{-1} of FeCo-PBA. This result thus indicates that a moderate APCP treatment might be able to serve as a simple but useful tool to enhance the intracellular utilization efficacy of nanoparticles, while reducing the NP doses. It is also clearly observed from the confocal *z*-tacking results (Fig. S9, ESI†) that plasma could not only enhance NP cellular uptake but also induce intercellular oxidative stress. Moreover, the higher the concentration of nanoparticles, the more nanoparticles a cell

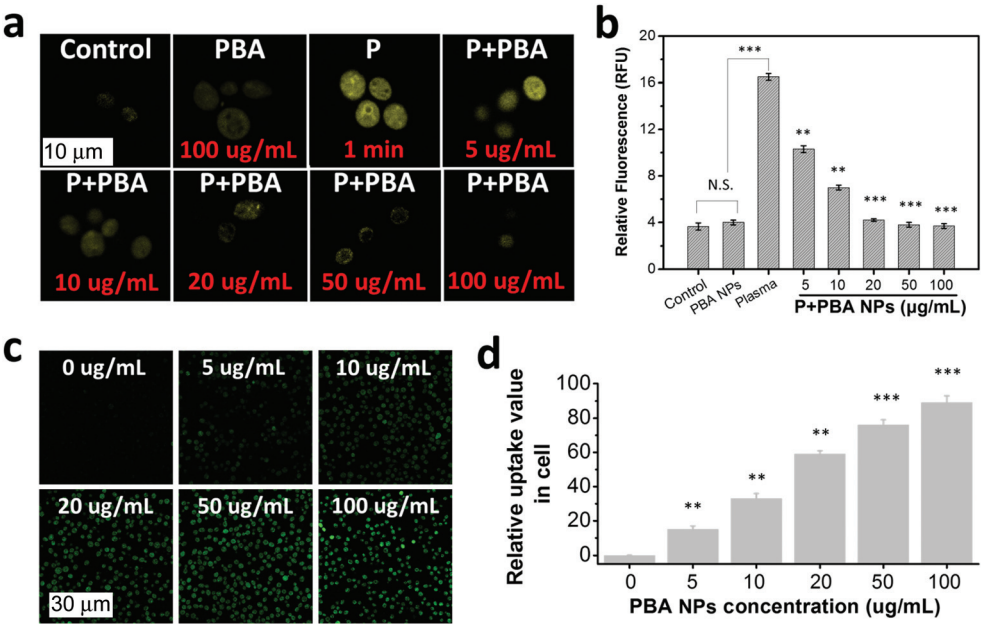

Fig. 4 (a) Fluorescence microscopy images of yeast cells incubated in different concentrations of PBA NP suspensions with and without plasma stress. (b) Intracellular ROS levels in yeast cells incubated in different concentrations of PBA NP suspensions with and without plasma stress. ROS intensity was expressed by relative fluorescence intensity. (c) Cellular uptake of plasma-stressed *S. cerevisiae* under different concentrations of PBA NPs. (d) NP uptake level was expressed by relative fluorescence intensity. The data points and error bars represent the averages and standard deviations from three independent measurements, respectively.

could take up. At the same time, the more the amount of nanoparticles a cell takes up, the lower the ROS level, which indicates that nanoparticles play the role of a ROS-scavenger.

Ethanol production efficiency of *S. cerevisiae* cells with FeCo-PBA NPs

During alcoholic fermentations, yeast cells are subjected to nutritional and environmental stress factors that may trigger the production of large amounts of ROS, affecting DNA, proteins, lipids, the cytoskeleton, and eventually cell survival.[27] Previous studies on ethanol toxicity have found that the fermentation product ethanol may also produce ROS (hydrogen peroxide and superoxide) *via* the generation of a hydroxyethyl radical, accumulated at the mitochondrial level and causing cellular damage.[27]

The ethanol yield of *S. cerevisiae* cells after 24 h of fermentation (glucose concentration: 120 g L^{-1}) with different amounts of FeCo-PBA NPs (0, 5, 10, 20, 50 and 100 μg mL^{-1}) is shown in Table 2. Importantly, the addition of FeCo-PBA NPs boosts the yield of ethanol. The lowest yield (14.93 g L^{-1}) is witnessed in the control group, where no FeCo-PBA NPs are added, and then the yields increase with increasing concentration of FeCo-PBA NPs in the culture broth. For example, 10 μg mL^{-1} of FeCo-PBA can increase ethanol production by 26%, and an ethanol concentration of 27.45 g L^{-1} (increased by more than 80%) is achieved when the dose of FeCo-PBA NPs is increased to 100 μg mL^{-1}.

The plasma-exposed cells are transferred into culture broths containing different doses of FeCo-PBA for ethanol production. Consistent with the previous reports, APCP itself can enhance the fermentation efficacy of yeast cells (by around 20%) in the anaerobic environment. Indeed, moderate plasma agitation may induce favourable phenotypic or even genotypic changes in the cells. These changes endow the cells with higher tolerance to stress generated during fermentation, quicker uptake of nutrients (such as glucose), and higher activity of enzymes involved in the metabolic pathways.[32,43]

The presence of PBA in the broth significantly increased ethanol production. To be specific, 5 μg mL^{-1} of FeCo-PBA increases the ethanol concentration to 22.67 g L^{-1} (increased by ~25.5%, compared to the value obtained under PBA free conditions), and the production is doubled (to 36.84 g L^{-1}) when 50 μg mL^{-1} of PBA is added. In the control group (without plasma treatment), the highest increment in ethanol production (by 83.86%) is obtained with the use of 100 μg mL^{-1} of PBA. Importantly, in the plasma-treated group, only 20 μg mL^{-1} is enough to achieve a comparative increment (85.25%). This result indicates that plasma treatment can significantly reduce the nanoparticle doses to achieve the same or even better results by boosting the cellular uptake of NPs, which is discussed later. The synergistic effects between the plasma and FeCo-PBA nanoparticles are also confirmed by the C-increment (derived by the comparison of the plasma group to the control group with the addition of the same amount of FeCo-PBA), which is always larger than 20.83%.

Upon plasma treatment, some changes in the cell membrane transport may arise due to the direct effect of the plasma (*e.g.*, electrons, ions, chemical reactive species, UV light, and moderate heat).[44] By altering the physico-chemical properties of the cell wall and membrane, the cells may attempt to regulate cross-membrane transport and thus prevent damage or withstand external forces from the stressor. Previous studies on CAP–cell interactions have reported pore formation in the cell membrane in response to CAP-generated chemically active species.[31,41,45] These species can induce chemical and physical changes on the biological surfaces; however, these changes in membrane permeability are generally transient.

Fig. 5 shows the oxidative stress response of the untreated and plasma-treated yeast cells fermented with different concentrations of FeCo-PBA NPs after fermentation. Compared to the ROS level before fermentation (Fig. S5, ESI†), which displays a dose-independent behaviour, a significant increase in fluorescence corresponding to the intracellular ROS concentration is observed after fermentation. This may be attributed to the fact that the fermentation-generated stress environment contributes to a noticeable increase in intracellular oxidative stress. On the other hand, the addition of PBA NPs at a concentration of 0–100 μg mL^{-1} can effectively inhibit intracellular ROS generation during fermentation, due to the cellular uptake of these nanoenzymes, acting as an intracellular ROS scavenger. All these results are consistent with those of cell viability and proliferation, indicating that PBA NPs may play a

Table 2 Ethanol concentration after 24 h of yeast anaerobic fermentation with different amounts of FeCo-PBA. The control group corresponds to yeast cells not treated with plasma. Mean values (± SE) for the respective triplicates are given

	Control group		1 min plasma pretreatment		
FeCo-PBA NPs (μg mL^{-1})	Ethanol (g L^{-1})	L-Increment[a] (%)	Ethanol (g L^{-1})	L-Increment[a] (%)	C-Increment[b] (%)
0	14.93 ± 1.61	—	18.04 ± 1.53	—	20.83
5	16.48 ± 0.73	10.38	22.67 ± 2.14	25.49	37.56
10	18.82 ± 1.04	26.05	28.55 ± 2.59	58.26	51.70
20	22.18 ± 1.34	48.56	33.42 ± 0.81	85.25	50.68
50	25.24 ± 2.56	69.06	36.84 ± 2.59	104.21	45.96
100	27.45 ± 2.64	83.86	37.96 ± 1.31	110.42	38.29

[a] The comparison to the yields obtained without adding FeCo-PBA (longitudinal comparison). [b] The comparison to the control group with the same amount of FeCo-PBA added (crosswise comparison).

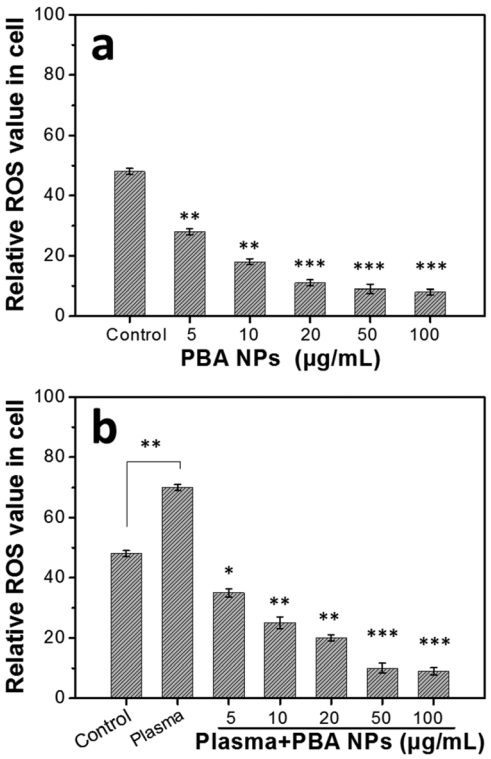

Fig. 5 Intracellular ROS levels in untreated (a) and plasma-treated (b) yeast cells incubated in different concentrations of PBA NP suspensions after fermentation. *S. cerevisiae* cells were cultured in YPD medium containing PBA NPs with the indicated concentrations (5–100 μg mL^{-1}). Cells were stained with the CellROX® Orange reagent for 30 min and observed by fluorescence microscopy (excitation wavelength: 545 nm, emission wavelength: 565 nm). ROS intensity was expressed by relative fluorescence intensity. The data points and error bars represent the averages and standard deviations from three independent experiments, respectively.

protective role against oxidative stress generated from alcoholic fermentation.

Experimental

Synthesis and characterization of FeCo-PBA nanoparticles

In a typical procedure, $Fe(NO_3)_2{\cdot}6H_2O$ (1.73 g, 6.0 mmol) and $K_3Co(CN)_6$ (1.33 g, 4.0 mmol) are dissolved in 200 mL deionized water respectively. Then the above two precursor solutions are mixed under magnetic stirring. The precipitates are collected by centrifugation, washed several times with distilled water and ethanol, and dried at 60 °C in a vacuum oven overnight. The crystalline phases of FeCo-PBA nanoparticles are characterized by X-ray powder diffraction (XRD, PANalytical X'Pert3) with Cu Kα radiation. Scanning electron microscopy (SEM, Tescan MIRA3) and high-resolution transmission electron microscopy (HRTEM, JEOL-2100, 200 kV) are employed to explore the size and morphology of the as-prepared samples. X-ray photoelectron spectroscopy (XPS, Kratos Axis) is used to identify the chemical composition and valence state of each element of the materials. Vibrational fingerprints of the chemical bonding of the nanoparticles are identified by Fourier transform infrared spectroscopy (FTIR, Nicoletis 50, ThermoFisher). Ultraviolet-visible (UV-VIS) absorption spectra are recorded on a UV-VIS-NIR spectrophotometer (UV-3600, Shimadzu, Japan).

Extracellular ROS scavenging activities of FeCo-PBA NPs

Catalase mimicking activity measurements. The elimination of H_2O_2 is investigated by measuring the fluorescence intensity. Phosphate buffered saline (PBS, 25 mM, pH 7.4) containing H_2O_2 (10 mM) and FeCo-PBA NPs (at a concentration of 0, 10 or 20 μg mL^{-1}) or anti-H_2O_2 reagents (10 U mL^{-1} of the natural catalase or 100 μM synthetic trolox) are mixed well and then incubated at 37 °C for 6 h. CellROX® Orange (5 μM, Life Technologies, Carlsbad, USA) is then added and incubated for another 30 min at room temperature, before measuring the fluorescence of the mixture. The elimination percentage for the quantitation of the ROS scavenging effect is calculated using the following equation: elimination (%) = $[(F_0 - F)/F_0] \times 100$, where F_0 is the fluorescence intensity of the group incubated either at room temperature or at 80 °C without the addition of any FeCo-PBA NPs and anti-ROS reagents (termed H_2O_2 only), while F represents the intensities of groups with scavengers. Three independent trials of the experiments are performed with the results shown as average ± standard deviation.

Measurement of SOD mimicking activity. $^{\bullet}O_2^-$ is generated and detected according to the literature.[35] Briefly, xanthine (X, 0.6 mM) and xanthine oxidase (XO, 0.05 U mL^{-1}) in phosphate buffer (0.1 M, pH 7.4) are incubated for 40 min at 37 °C for the preparation of $^{\bullet}O_2^-$ containing solutions, and $^{\bullet}O_2^-$ is then characterized using its specific fluorescent probe hydroethidine (0.5 mg mL^{-1}), which can be oxidized by $^{\bullet}O_2^-$ into ethidium with the excitation and emission wavelengths at 470 and 610 nm, respectively. For $^{\bullet}O_2^-$ scavenging, 10 or 20 μg mL^{-1} of FeCo-PBA NPs, or anti-$^{\bullet}O_2^-$ reagents (2 U mL^{-1} of the natural superoxide dismutase (SOD) or 1 mM synthetic agent tempol) is added and incubated at 37 °C for 6 h. The amount of $^{\bullet}O_2^-$ scavenged is then determined again by measuring the fluorescence intensity. The calculation of $^{\bullet}O_2^-$ elimination is the same as that of H_2O_2.

Thermal stability tests. FeCo-PBA and the anti-ROS reagents (natural enzymes, catalase and SOD, and trolox/tempol) are pre-treated for 1 h at 80 °C respectively, before being used to scavenge H_2O_2 and $^{\bullet}O^{2-}$ to compare their thermal stability for ROS scavenging.

Yeast strains and plasma treatment

S. cerevisiae AWRI 1631 is a haploid strain, provided by the Australian Wine Research Institute. It is routinely maintained in a basic YPD agar/medium, which consists of the following (g L^{-1}): yeast extracts 10, bacteriological peptone 20, glucose 20, with/without agar 15. *S. cerevisiae* cells are cultured on agar plates at 37 °C and allowed to grow for 72 h before APCP treatment.[32] Individual colonies of similar size are then subjected to direct APCP exposure for different durations (Fig. S2, ESI†). Plasma is generated using an atmospheric pressure plasma jet

(kINPen08, 1.7 MHz, 2–6 kV), and argon (Ar) is used as the feed gas at a flow rate of 5 standard litres per minute (SLM). The distance between the jet nozzle and yeast colonies is constant (~7 mm). More details about the description of this type of plasma jet and biological sample treatment can be found in our previous studies.[32] For the control group, only 5 SLM of Ar gas is fed (without the voltage added) and used for the same treatment time for comparison.

Incubation of yeast cells and fermentation with PBA NPs

Fresh YPD medium is used to prepare the Fe–Co PBA NP containing solution at a concentration of 2000 μg mL^{-1}. After being sonicated for 30 min (AS3120, Autoscience, China), the stock solution is ready to be applied in yeast incubation and fermentation. Before cell viability tests, the treated or control colonies are transferred into YPD media and seeded at a density of 5000 cells per well in 96-well plates, incubated with or without PBA NPs of different concentrations for 1 h. Cell viability was assessed by staining the cells with methylene blue (0.1 mg mL^{-1} stock solution, dissolved in a 2% dehydrated sodium citrate solution).[32] Cell growth assay is performed using a microplate reader (Bio-Rad 680, USA) at an absorbance of 600 nm for 24 h.

To test the yeast fermentation efficacy with or without FeCo-PBA, a modified YPD medium (containing 120 g L^{-1} glucose, which is the only difference compared to pristine YPD) is employed, and PBA in the stock solution is added to the required concentrations. Culture media (30 mL) are then incubated under anaerobic isothermal conditions and at 30 °C for 2 days. More details about the experimental procedure are shown in Fig. S1, ESI.† All fermentation experiments are performed in triplicate.

Ethanol determination. Ethanol production is analyzed with the ethanol assay kit (Megazyme, Ireland) according to the manufacturer's protocol. 100 μL sample solution, which is diluted 1000 times, mixed with 200 μL distilled water, 20 μL solution 1 (buffer), 20 μL solution 2 (nicotinamide-adenine dinucleotide, NAD^+) and 5 μL solution 3 (aldehyde dehydrogenase, AIDH), is placed at room temperature for a reaction time of 5 min and measured with a microplate reader at a wavelength of 340 nm. The reactions are then started by the addition of 2 μL suspension 4 (alcohol dehydrogenase, ADH) and the absorbance is continuously read at 1 min intervals until the absorbance increases constantly over 1 min. Absorbance values are calibrated using a single point standard solution diluted properly when highly concentrated using the same batch of reagents. The calculation (Microplate Assay Procedure) is:

$$\text{Ethanol yield (g L}^{-1}) = \frac{\Delta A_{\text{sample}}}{\Delta A_{\text{standard}}} \times \text{standard concentration} \times F$$

where F is the dilution factor of the sample solution.

Intracellular ROS detection. Intracellular ROS generation is again determined using the CellROX® Orange reagent according to the manufacturer's instructions. The CellROX® Orange reagent is an ideal fluorogenic probe for measuring oxidative stress in live cells.[32] This cell-permeant dye is non-fluorescent, while in a the reduced state it exhibits bright fluorescence due to oxidation by ROS. The cells are analysed using a Promega GloMax plate reader at an excitation and emission wavelength of 545 and 565 nm, respectively.

Statistical analysis. Results are expressed as mean ± SD (range) or a percentage value. Comparisons between groups were made using Student's unpaired t-test. Statistical significance of P-values was represented. $^*p < 0.05$, $^{**}p < 0.01$, $^{***}p < 0.001$, $^{****}p < 0.0001$. All calculations were performed using the GraphPad Prism software package (GraphPad Software Inc., San Diego, CA, USA).

Conclusions

In summary, we synthesize Prussian Blue Analogue (PBA) nanoparticles (nanoenzymes) with good biocompatibility and ROS scavenging ability. The PBA nanoenzymes are successfully used in the conversion of glucose into ethanol during yeast fermentation, the efficacy of which depends mainly on the yeast's ability to counteract the stress factors during the process. Our results show that the PBA NPs can protect cells from oxidative stress induced by both plasma exposure and fermentation processes. As a result, the secondary metabolite yields and energy production are improved. This work confirms the positive effects of PB-based NPs in living cells and their ROS scavenging ability, vitally needed for the development of next-generation nanotechnology-enabled oxidative stress mediators for diverse applications in biotechnology and biomedicine.

Conflicts of interest

The authors declare no competing financial interest.

Acknowledgements

This work was partially supported by the Australian Research Council (ARC). The Translational Research Institute (TRI) receives funding from the Australian Government. We acknowledge support from the Central Analytical Research Facility operated by the Institute of Future Environment (QUT). The authors would also like to thank Mr Rusen Zhou for his kind assistance in manuscript revision.

Notes and references

1 B. Yang, Y. Chen and J. Shi, *Chem. Rev.*, 2019, **119**, 4881–4985.
2 B. D'Autréaux and M. B. Toledano, *Nat. Rev. Mol. Cell Biol.*, 2007, **8**, 813.

3 B. C. Dickinson and C. J. Chang, *Nat. Chem. Biol.*, 2011, **7**, 504.
4 C. Nathan and A. Cunningham-Bussel, *Nat. Rev. Immunol.*, 2013, **13**, 349.
5 H. Guo, J. B. Callaway and J. P. Ting, *Nat. Med.*, 2015, **21**, 677.
6 Q. Cui, J. Wang, Y. G. Assaraf, L. Ren, P. Gupta, L. Wei, C. R. Ashby Jr., D. Yang and Z. Chen, *Drug Resist. Updates*, 2018, **41**, 1–25.
7 H. Jia, D. Yang, X. Han, J. Cai, H. Liu and W. He, *Nanoscale*, 2016, **8**, 5938–5945.
8 X. Wang, X. J. Gao, L. Qin, C. Wang, L. Song, Y. Zhou, G. Zhu, W. Cao, S. Lin and L. Zhou, *Nat. Commun.*, 2019, **10**, 704.
9 S. Nakajima, I. Ohsawa, K. Nagata, S. Ohta, M. Ohno, T. Ijichi and T. Mikami, *Behav. Brain Res.*, 2009, **200**, 15–21.
10 J. M. Matés, C. Pérez-Gómez and I. N. De Castro, *Clin. Biochem.*, 1999, **32**, 595–603.
11 R. Breslow, *Acc. Chem. Res.*, 1995, **28**, 146–153.
12 P. V. Iyer and L. Ananthanarayan, *Process Biochem.*, 2008, **43**, 1019–1032.
13 S. R. Doctrow, K. Huffman, C. B. Marcus, W. Musleh, A. Bruce, M. Baudry and B. Malfroy, *Advances in Pharmacology*, Elsevier, 1996, vol. 38, pp. 247–269.
14 B. J. Day, *Biochem. Pharmacol.*, 2009, **77**, 285–296.
15 C. Ge, G. Fang, X. Shen, Y. Chong, W. G. Wamer, X. Gao, Z. Chai, C. Chen and J.-J. Yin, *ACS Nano*, 2016, **10**, 10436–10445.
16 H. Wei and E. Wang, *Chem. Soc. Rev.*, 2013, **42**, 6060–6093.
17 J. Wu, X. Wang, Q. Wang, Z. Lou, S. Li, Y. Zhu, L. Qin and H. Wei, *Chem. Soc. Rev.*, 2019, **48**, 1004–1076.
18 B. Liu and J. Liu, *Nano Res.*, 2017, **10**, 1125–1148.
19 B. Liu and J. Liu, *Nanoscale*, 2015, **7**, 13831–13835.
20 F. Yang, S. Hu, Y. Zhang, X. Cai, Y. Huang, F. Wang, S. Wen, G. Teng and N. Gu, *Adv. Mater.*, 2012, **24**, 5205–5211.
21 L. Jing, X. Liang, Z. Deng, S. Feng, X. Li, M. Huang, C. Li and Z. Dai, *Biomaterials*, 2014, **35**, 5814–5821.
22 L. Su, Y. Xiong, H. Yang, P. Zhang and F. Ye, *J. Mater. Chem. B*, 2016, **4**, 128–134.
23 W. Zhang, S. Hu, J.-J. Yin, W. He, W. Lu, M. Ma, N. Gu and Y. Zhang, *J. Am. Chem. Soc.*, 2016, **138**, 5860–5865.
24 M. Shokouhimehr, E. S. Soehnlen, J. Hao, M. Griswold, C. Flask, X. Fan, J. P. Basilion, S. Basu and S. D. Huang, *J. Mater. Chem.*, 2010, **20**, 5251–5259.
25 D. Aguila, Y. Prado, E. S. Koumousi, C. Mathoniere and R. Clérac, *Chem. Soc. Rev.*, 2016, **45**, 203–224.
26 M. Vázquez-González, R. M. Torrente-Rodríguez, A. Kozell, W.-C. Liao, A. Cecconello, S. Campuzano, J. M. Pingarrón and I. Willner, *Nano Lett.*, 2017, **17**, 4958–4963.
27 R. V. Perez-Gallardo, L. S. Briones, A. L. Díaz-Pérez, S. Gutiérrez, J. S. Rodríguez-Zavala and J. Campos-García, *FEMS Yeast Res.*, 2013, **13**, 804–819.
28 J. Guo, M. Suástegui, K. K. Sakimoto, V. M. Moody, G. Xiao, D. G. Nocera and N. S. Joshi, *Science*, 2018, **362**, 813–816.
29 H. Alper, J. Moxley, E. Nevoigt, G. R. Fink and G. Stephanopoulos, *Science*, 2006, **314**, 1565–1568.
30 C. Willyard, *Nature*, 2017, **542**, 406.
31 J. Van der Paal, E. C. Neyts, C. C. Verlackt and A. Bogaerts, *Chem. Sci.*, 2016, **7**, 489–498.
32 N. Recek, R. Zhou, R. Zhou, V. S. J. Te'o, R. E. Speight, M. Mozetič, A. Vesel, U. Cvelbar, K. Bazaka and K. K. Ostrikov, *Sci. Rep.*, 2018, **8**, 8252.
33 R. Sharma, M. A. Iqubal, S. Jheeta and Kamaluddin, *Inorganics*, 2017, **5**, 18.
34 F. Zheng, D. Zhu, X. Shi and Q. Chen, *J. Mater. Chem. A*, 2015, **3**, 2815–2824.
35 J. Yao, Y. Cheng, M. Zhou, S. Zhao, S. Lin, X. Wang, J. Wu, S. Li and H. Wei, *Chem. Sci.*, 2018, **9**, 2927–2933.
36 Q. Mu, G. Jiang, L. Chen, H. Zhou, D. Fourches, A. Tropsha and B. Yan, *Chem. Rev.*, 2014, **114**, 7740–7781.
37 R. Zhou, R. Zhou, P. Wang, B. Luan, X. Zhang, Z. Fang, Y. Xian, X. Lu, K. Ostrikov and K. Bazaka, *ACS Appl. Mater. Interfaces*, 2019, DOI: 10.1021/acsami.9b03961, in press.
38 R. Zhou, R. Zhou, F. Yu, D. Xi, P. Wang, J. Li, X. Wang, X. Zhang, K. Bazaka and K. K. Ostrikov, *Chem. Eng. J.*, 2018, **342**, 401–409.
39 R. Zhou, R. Zhou, K. Prasad, Z. Fang, R. Speight, K. Bazaka and K. K. Ostrikov, *Green Chem.*, 2018, **20**, 5276–5284.
40 F. Dong, J. Zhang, K. Wang, Z. Liu, J. Guo and J. Zhang, *Nanoscale*, 2019, **11**, 1123–1130.
41 K. Prasad, N. Recek, R. Zhou, R. Zhou, M. Aramesh, A. Wolff, R. Speight, M. Mozetič, K. Bazaka and K. K. Ostrikov, *Sustainable Mater. Technol.*, 2019, **22**, e00123.
42 N. Recek, X. Cheng, M. Keidar, U. Cvelbar, A. Vesel, M. Mozetic and J. Sherman, *PLoS One*, 2015, **10**, e0119111.
43 X. Zhang, X. F. Zhang, H. P. Li, L. Y. Wang, C. Zhang, X. H. Xing and C. Y. Bao, *Appl. Microbiol. Biotechnol.*, 2014, **98**, 5387–5396.
44 H. Li, W. Sun and K. Ostrikov, *Phys. Rep.*, 2018, **770–772**, 1–45.
45 A. Bogaerts, M. Yusupov, J. Razzokov and J. Paal, *Front. Chem. Sci. Eng.*, 2019, **13**, 253–263.